Accepted for publication in ***Computers & Fluids***, March 2013

Quality assessment of Large-Eddy Simulation of wind flow around a high-rise building: validation and solution verification

P. Gousseau [*(a)], *B. Blocken* [(b)], *G.J.F. van Heijst* [(c)]

(a) *Building Physics and Services, Department of the Built Environment, Eindhoven University of Technology, P.O. Box 513, 5600 MB Eindhoven, The Netherlands, p.gousseau@tue.nl*

(b) *Building Physics and Services, Department of the Built Environment, Eindhoven University of Technology, P.O. Box 513, 5600 MB Eindhoven, The Netherlands, b.j.e.blocken@tue.nl*

(c) *Fluid Dynamics Laboratory, Department of Applied Physics, Eindhoven University of Technology, P.O. Box 513, 5600 MB Eindhoven, The Netherlands, g.j.f.v.heijst@tue.nl*

Abstract

When undertaking wind engineering problems such as urban pollutant dispersion or pedestrian wind comfort with Computational Fluid Dynamics, an accurate simulation of the flow-field around buildings is required. In this respect, the good performance of Large-Eddy Simulation has already been established but because the formulation and the use of this turbulence modeling approach are complex, the uncertainty on the results is relatively high. This implies the need for validation and verification (V&V) studies like the one performed in the present paper for the wind flow around an isolated high-rise building with aspect ratio 1:1:2. In the first part of the study, the numerical results are compared with measurements from a reference wind-tunnel experiment and the agreement is quantified by validation metrics. The vortex method to generate inflow turbulence is shown to provide accurate results. Unexpectedly, the best agreement with the experiments is obtained on the coarsest computational grid, with 20 cells per building side, while a finer grid with 30 cells per building side over-estimates the turbulent kinetic energy measurements. A similar result was also found by earlier studies for different flow configurations. In the second part of the study, solution verification is performed. The Systematic Grid and Model Variation technique is used to provide estimates of the modeling and numerical error contributions. The *LES_IQ* indicator shows that a grid with 20 (resp. 30) cells per building side allows resolving 80% (resp. 91%) of the total turbulent kinetic energy in the region around the building.

Keywords:

Computational Fluid Dynamics (CFD); Validation and Verification (V&V); Urban wind flow; Large-Eddy Simulation (LES); Turbulence modeling; Bluff body aerodynamics.

1. Introduction

Computational Fluid Dynamics (CFD) is increasingly used to solve wind engineering problems such as pollutant dispersion in the built environment, pedestrian wind comfort, wind loads on buildings or natural ventilation of buildings (Hanna et al., 2006; Yoshie et al., 2007; Nozu et al., 2008; van Hooff et al. 2011; Blocken et al., 2012; Ramponi and Blocken, 2012). In all these cases, an accurate simulation of the wind flow around buildings by the CFD model is needed. This is the reason why – supported by the increase of computational power – the use of the Large-Eddy Simulation (LES) turbulence modeling approach is

* **Corresponding author**: Pierre Gousseau, Building Physics and Services, Eindhoven University of Technology, P.O. Box 513, 5600 MB Eindhoven, The Netherlands. *Tel*: +31 (0)40 247 4374. *Fax*: +31 (0)40 243 8595. *E-mail address:* p.gousseau@tue.nl

nowadays becoming more widespread in Computational Wind Engineering (CWE). Several earlier studies (Murakami, 1993; Rodi, 1997; Shah and Ferziger, 1997; Tominaga et al., 2008a), have indeed demonstrated that LES can provide an accurate description of the mean and instantaneous flow-field around bluff bodies like buildings. In general, it performs better than the Reynolds-Averaged Navier-Stokes (RANS) turbulence modeling approach, at the expense of much larger requirements in terms of computational resources.

Most of the aforementioned studies have established the good performance of LES based on comparison of the numerical results with measurements, often provided by wind-tunnel experiments. However, despite the increasing attention given to the quantification of error and uncertainty in CFD, the techniques that have been developed for general fluid engineering problems to assess the quality of CFD simulations are still marginally used in CWE (Franke, 2010). This is particularly true for LES.

The aim of the present study is to provide a Validation and Verification (V&V) study of the LES computation of wind flow around an isolated building. To the best of the authors' knowledge, this V&V strategy that has been developed for general fluid engineering problems has not yet been applied to such a flow.

Validation is defined as "the process of determining the degree to which a model is an accurate representation of the real world from the perspectives of the intended uses of the model" (AIAA, 1998). It will be performed here by comparing the numerical results with the measurements from a reference wind-tunnel experiment and by quantifying the agreement with validation metrics (Section 4). The influence of the subgrid-scale (SGS) model and grid resolution will be assessed. In particular, the results of simulations without SGS model, with the standard Smagorinsky SGS model and with its dynamic version will be compared. For the standard Smagorinsky model, an appropriate value for the Smagorinsky coefficient will be determined in what is usually referred to as "calibration" in the V&V process (AIAA, 1998).

Verification is defined as "the process of determining that a model implementation accurately represents the developer's conceptual description of the model and the solution to the model" (AIAA, 1998). Note that other definitions for the terms "validation" and "verification" can be found for example in (Casey and Wintergerste, 2000) or (Srebric and Chen, 2002). The process of verification is twofold: on the one hand the code verification and on the other hand the solution verification (AIAA, 1998; Roache, 1998; Oberkampf and Trucano, 2002) The former will not be treated here: the CFD code used is a commercial code (Ansys/Fluent 12.1) and is assumed to be verified in the development process. The solution verification will be performed in four steps:

(1) Evaluating the turbulent inflow generation technique. Here, the Vortex Method (VM) (Sergent, 2002; Mathey et al., 2006) is used. Besides testing the influence of inflow turbulence on the flow field around the building (validation), a-posteriori verification will be performed indicating that the mean inflow is a good representation of the experimental one (Section 4.1).
(2) Assessing the statistical convergence of the numerical solution. The LES results are compared to the measurements in terms of mean values. It will be verified that the first moments of velocity are sufficiently converged (Section 5.1).
(3) Evaluating the modeling and numerical error contributions in the LES solution. For basic flows at low Reynolds numbers, this can be achieved using Direct Numerical Simulation (DNS) results (Vreman et al., 1996; Geurts and Fröhlich, 2002; Meyers et al., 2003). However, in the present study the high Reynolds number of the flow prohibits the application of DNS so a multi-grid technique is used: the Systematic Grid and Model Variation (SGMV) (Klein, 2005; Freitag and Klein, 2006; Klein et al., 2008; Celik et al., 2009) (Section 5.2).
(4) Evaluating the proportion of the total turbulent kinetic energy which is resolved by the LES model with the LES Index of Quality (*LES_IQ*) (Celik et al., 2005; Celik et al., 2006; Celik et al., 2009) (Section 5.3).

The reference experiment that will be reproduced with CFD is described in the next section. Next, the computational model is outlined, before presenting and analyzing the results.

2. Description of the experiment

The wind-tunnel experiment by Meng and Hibi (1998) is used as a validation experiment. A building with dimensions $b \times b \times h$ ($b=h/2=0.08$m) in the streamwise (x), lateral (y) and vertical (z) direction, respectively, is placed in the test section of a wind tunnel where an Atmospheric Boundary Layer (ABL) flow is simulated. The Reynolds number based on b and the mean velocity of the incident flow at building height (U_h) is equal to 2.4×10^4. The origin of the coordinate system is the center of the building's ground face. The streamwise turbulence intensity at $z/b=0.125$, 2 and 7.5 is equal to 22.8%, 18% and 4.5%, respectively. The undisturbed ABL profiles of mean streamwise velocity ($U=\langle u \rangle$), standard deviation of velocity in the three directions (σ_u, σ_v, σ_w) and shear stress ($-\langle u'w' \rangle$, where $u_i'=u_i-U_i$ denotes the fluctuation of the velocity in the direction x_i) are provided in the experimental report.

The mean (U, V, W) and standard deviation of the three velocity components have been measured with a constant-temperature anemometer with split-fiber probe at 186 points around the building. 66 of these points are in the vertical mid-plane $y/b=0$, hereafter denoted by V0. Two horizontal planes at $z=1$cm (H1; $z/b=0.125$) and $z=10$cm (H10; $z/b=1.25$) contain 60 additional measurement points each. In each plane, the points are distributed along 9 lines at $x/b=-0.75$; -0.5; -0.25; 0; 0.5; 0.75; 1.25; 2; 3.25. Because of space limitations, the graphical comparison (profiles) of experimental and numerical data will be performed only in the planes V0 and H10 for a limited number of points (5 out of 9 measurement lines per plane) and variables (U and the turbulent kinetic energy $k=0.5\times(\sigma_u^2+\sigma_v^2+\sigma_w^2)$). The validation metrics, however, take into account all the data points. Note that this experiment has been reproduced with CFD before by Tominaga et al. (2008a); their LES results will also be used in our study for comparison purposes.

3. Computational model

3.1. LES modeling

The commercial CFD code Ansys Fluent 12.1 is used here, with LES as a turbulence modeling approach. The filtered incompressible Navier-Stokes equations are given by:

$$\frac{\partial \bar{u}_i}{\partial x_i} = 0 \tag{1}$$

$$\frac{\partial \bar{u}_i}{\partial t} + \bar{u}_j \frac{\partial \bar{u}_i}{\partial x_j} = -\frac{1}{\rho}\frac{\partial \bar{p}}{\partial x_i} + \frac{\partial}{\partial x_j}\left(\nu \frac{\partial \bar{u}_i}{\partial x_j}\right) - \frac{\partial \tau_{ij}}{\partial x_j} \tag{2}$$

where the overbar denotes the filtering operator (with filter width equal to grid size), ρ and ν are the air density and kinematic viscosity, respectively, p the pressure and τ_{ij} the components of the SGS stress tensor:

$$\tau_{ij} = \overline{u_i u_j} - \bar{u}_i \bar{u}_j \tag{3}$$

Two simulations will be run without any subgrid-scale model, i.e. by omitting the last term on the right-hand side of Eq. 2. The intention is to observe whether the dissipation due to the numerical scheme used here can mimic the effect of the smallest scales of motion. For the other simulations, the Smagorinsky SGS model (Smagorinsky, 1963) is applied to close the system of equations and determine

the SGS stresses via the SGS turbulent viscosity v_{SGS} and the filtered rate of strain $\overline{S_{ij}}$ =($\partial\bar{u}_i/\partial x_j+\partial\bar{u}_j/\partial x_i$)/2:

$$\tau_{ij} - \frac{1}{3}\tau_{kk}\delta_{ij} = -2\nu_{SGS}\overline{S}_{ij} \tag{4}$$

with:

$$\nu_{SGS} = L_{SGS}^2\overline{S} \tag{5}$$

where $\overline{S} = \left(2\overline{S_{ij}}\,\overline{S_{ij}}\right)^{1/2}$ is the characteristic filtered rate of strain and L_{SGS}=min(κd,$C_s V_c^{1/3}$) is the SGS mixing length, with κ the von Karman constant, d the distance to the closest wall, V_c the volume of the computational cell and C_s the Smagorinsky coefficient. Note that Eq. (2) corresponds to the momentum equation filtered with a uniform filter width and the commutation error that arises when filtering the equation on a non-uniform grid is neglected (Moin et al., 1978; Ghosal and Moin, 1995; Vasilyev et al., 1998).

The distinction is made here between the so-called standard Smagorinsky model, where C_s is a user-prescribed constant, and the dynamic version (Germano et al., 1991; Lilly, 1992), where C_s is computed at each time step with a test-filter (whose width is twice the grid size) and clipped to the range [0; 0.23] to avoid numerical instabilities. The upper bound of this range aims at preventing the appearance of extremely high C_s values which, on the one hand, are not physical and, on the other hand, can lead to high spatial variations of C_s and destabilize the solver. The imposed maximum value for C_s ($C_{s,max}$) should be high enough to allow the description of all types of flow, but the particular value imposed is different in each CFD code, showing that there is no widely-accepted value for $C_{s,max}$. Here, $C_{s,max}$=0.23 is used, which is the default value in Ansys Fluent 12.1 (Ansys Inc., 2009). The two versions of the Smagorinsky model will be used and compared in the present study. For the standard version, two different values of C_s will be tested: 0.1 and 0.15. They belong to the range of values that can be found in the literature for the simulation of flow around a bluff body, e.g. 0.1 in (Rodi et al., 1997; Rodi, 1997; Thomas and Williams, 1997; Lim et al., 2009; Xie and Castro, 2009), 0.12 in (Murakami, 1993; Tominaga et al., 2008a; Tominaga and Stathopoulos, 2010; Tominaga and Stathopoulos, 2011), or 0.16 in (Tseng et al., 2006). Note that the simulations with these two model coefficients will be used in the solution verification procedure to evaluate the modeling error (Section 5.2).

3.2. Computational domain and grid

The computational domain has been created and meshed with the Gambit software following the surface-extrusion technique (van Hooff and Blocken, 2010). The domain dimensions are 2.64×0.9×0.9 m^3 (Fig. 1a), with a distance of 4h between the inflow boundary and the windward facade of the building. This value is set slightly below the recommendations by COST Action 732 (Franke et al., 2007) and AIJ (Tominaga et al., 2008b) guidelines in order to limit the deterioration of the prescribed inflow profiles along the empty fetch upstream of the building (Blocken et al., 2007a; Blocken et al., 2007b). In the vertical direction, the height of the wind-tunnel test section is used (0.9m=5.625h) and the top wall boundary is modeled. To avoid modeling the side-walls of the wind tunnel (which would require grid refinement and increase the total number of cells significantly), the width of the domain has been chosen slightly smaller than the test-section width (0.9m=11.25b vs. 1.1m). Nevertheless, this dimension implies an empty distance of 5.125b on each side of the building, which ensures a small influence of the side boundary conditions on the flow around the building. The resulting blockage ratio is equal to 1.6%, which

is below the maximum values recommended by the aforementioned guidelines (Franke et al., 2007; Tominaga et al., 2008b).

Two computational grids are used in this study, namely Grid20 and Grid30. The suffix corresponds to the number of cells used to discretize the building in the x- and y-directions. The same uniform grid spacing is applied on the building in the vertical direction. Away from the building, the cell size is increased by a factor kept around 1.08 to limit the commutation error. Note that the resulting high aspect ratio of the computational cells in some regions of the domain is not optimal for LES (using cubic cells is generally advised) but appears to be inevitable for applied cases with complex geometries (Gousseau et al., 2011a). The characteristics of the two grids are summarized in Table 1 and the grid on the building and ground surfaces for Grid20 is shown in Figs. 1b,c. As will be explained later (Section 5), the solution verification methods used here are based on the numerical solutions of the LES equations on these two grids. An important parameter in this procedure is the grid coarsening factor $\alpha=\Delta_{20}/\Delta_{30}$, equal to the ratio of the coarse filter width/cell size (Δ_{20}) and the fine one (Δ_{30}). Ideally, α should be kept constant everywhere in the domain. This is straightforward in the case of a uniform grid but in the case of more complex grid systems like the one used here, special care must be taken to achieve this. As an example, the evolution of Δ_{20}, Δ_{30} and α along two lines crossing the domain is shown in Fig. 2. For geometrical reasons, deviations from the intended value (α=1.5 imposed at the building) are inevitable but they have been kept very limited.

3.3. Boundary conditions

Symmetry boundary conditions are imposed at the sides of the domain (y=±0.45m), implying zero normal velocity and zero gradients of all variables at these boundaries. At the outlet of the domain, zero static pressure is imposed.

The building and ground surfaces as well as the top boundary of the domain are defined as walls. The centroids of the wall-adjacent cells are assumed to lie either in the linear sub-layer, in the buffer layer or in the logarithmic zone of the boundary layer, depending on the distance to the wall (Ansys Inc., 2009). For Grid20, z^+ values ($z^+=zu_\tau/\nu$, where $u_\tau=(\tau_w/\rho)^{1/2}$ is the friction velocity with τ_w the wall shear stress) at the centroids of the wall-adjacent cells reach values up to 50 at the ground, 75 at the building surface and 225 at the ceiling. Note that no special treatment has been applied to the ground surface to take into account its roughness but the inflow boundary is located close enough to the building to limit the appearance of longitudinal gradients in the ABL profiles (Blocken et al., 2007a; Blocken et al., 2007b). This has been verified by looking at the flow at a point P located at the same streamwise position as the windward facade of the building but relatively far from it in the lateral direction, in such a way that the ABL flow is not disturbed by the presence of the building. P is the point of non-dimensional coordinates (x/b=-0.5; y/b=3.75; z/b=2), i.e. the point located at building height, at the level of the windward facade, 3.25b away from the side wall. At P, the deviations from the prescribed inlet values of U and k at building height are equal to 1% and 5%, respectively, showing the good homogeneity of the prescribed profiles along the empty fetch upstream of the building.

Since LES is an unsteady model, the velocity profile imposed at the inlet of the domain must be time-dependent. Several techniques exist to achieve this, see for example (Tamura, 2008; Yoshie et al., 2011) for a review. Here it has been chosen to use the Vortex Method (VM) (Sergent, 2002; Mathey et al., 2006). It consists in generating and transporting randomly in the inlet plane a given number (here: 200) of 2D-vortices whose intensity and size depends on the local value of k and the turbulence dissipation rate, for which profiles are prescribed based on the experiment. The turbulence dissipation rate is calculated assuming equilibrium between production and dissipation of turbulent kinetic energy in the ABL flow. The vortices generate unsteady perturbations v_{in}' and w_{in}' on the prescribed profiles of V and W, respectively. The perturbations u_{in}' on the imposed profile of U are deduced from v_{in}' and w_{in}' following $u_{in}'=-\vec{v}'.\vec{e}$ where $\vec{v}'$ is the vector of components (0;v_{in}';w_{in}') and $\vec{e}$ is the unit vector aligned with the gradient of mean velocity in the inlet plane. The advantage of this method is that it requires

neither additional simulation nor extra domain length. This technique has been used in earlier studies by the authors (Gousseau et al., 2011a; Gousseau et al., 2011b; Gousseau et al., 2012) and showed good performance in LES of pollutant dispersion around buildings. Here, the accuracy and relevance of the VM will be analyzed in more detail (Section 4.1).

3.4. Numerical procedure

The bounded central-differencing scheme is used to discretize the convection term in the filtered momentum equation. In comparison with pure central-differencing, this scheme switches to first-order upwind scheme when the convection boundedness criterion (Gaskell and Lau, 1988) is violated, which avoids the appearance of unphysical oscillations in the numerical solution. It has an order of accuracy between one and two. From the pressure values at the cell centers, the face values are computed with a second-order scheme. Pressure-velocity coupling is performed with the fractional step method (Kim and Moin, 1985; Bell et al., 1989).

Time discretization is second-order implicit. The non-iterative scheme is used for time advancement: each set of equations is solved iteratively but not in combination, which decreases the computational time significantly. First, for the momentum equations, sub-iterations are performed within each time step until the ratio of the residual at the current sub-iteration and at the first sub-iteration of the time step is less than 0.05. Then, sub-iterations are performed on the pressure correction equation until the residual has decreased by a factor 0.25. Convergence monitoring shows that these thresholds are generally reached by performing 2 to 3 sub-iterations for each equation. Note that the individual contribution of the iteration error has not been evaluated but is included in the numerical error computed in Section 5.2.

The time-step value (Δt) has been adapted for each computational grid: it is equal to 8×10^{-4}s for Grid20 and 5.33×10^{-4}s for Grid30, corresponding to 0.045 and 0.03 time units ($t_u=b/U_h$), respectively. Similar values for the Courant number ($=u\times\Delta t/h_c$, with u the local velocity value and h_c the local cell size) are therefore found on both grids, the maximum on the whole domain being approximately 2.3. Each simulation is initialized with the solution of a preceding RANS simulation on which random noise is super-imposed. After an initialization period T_{init}=3.2s corresponding to 5.4 flow-through times ($T_{ft}=L_x/U_h$, where L_x is the length of the computational domain), the statistics are sampled for T_{avg}=12.8s=21.8T_{ft}=718t_u. It will be demonstrated in Section 5.1 that this averaging period is sufficiently long to provide converged mean values of velocity.

3.5. List of cases

The name and description of the seven cases that will be presented in this article are summarized in Table 2.

The simulations have been run in parallel on eight processors (2.33GHz; 64GB memory). In total the LES20-1 simulation lasted approximately 30 hours, including the initialization phase. The use of the dynamic Smagorinsky model (LES20-3) did not strongly increase the computational time (ratio 1.15:1). Because of the increase in number of time steps and in computational time per time step, the simulations on Grid30 demanded significantly more time to run on the same computer system (ratio 6:1 for LES30-1 compared to LES20-1).

To quantify the agreement between numerical and experimental results, validation metrics are used in the next section and reported in Table 3 for U, V, W and k: hit-rate (q) and fraction of predictions within a factor of 2 of observations (*FAC2*). In addition for k, the Fractional Bias (*FB*) and Normalized Mean Square Error (*NMSE*) are used. The values take into account all the 186 measurement points and, except for the hit rate, they have been calculated with the BOOT software (www.harmo.org, 2012). The ideal value of each metric, corresponding to perfect agreement between CFD and experiment, is indicated in the second line of Table 3. The definitions of these metrics are given hereafter (Schatzmann et al., 2010):

Hit rate (q):

$$q=\frac{1}{N}\sum_{i=1}^{N} n_i \quad \text{with} \quad n_i=\begin{cases}1 & \text{for } \left|\frac{P_i-O_i}{P_i}\right|\le D_q \text{ or } |P_i-O_i|\le W_q \\ 0 & \text{else}\end{cases} \tag{6}$$

Fraction of predictions within a factor of 2 of observations (*FAC2*):

$$FAC2=\frac{1}{N}\sum_{i=1}^{N} n_i \quad \text{with} \quad n_i=\begin{cases}1 & \text{for } 0.5\le\frac{P_i}{O_i}\le 2 \\ 0 & \text{else}\end{cases} \tag{7}$$

Fractional bias (*FB*):

$$FB=FB_{fn}-FB_{fp} \quad \text{with} \quad FB_{fn}=\frac{[O]_{fn}-[P]_{fn}}{0.5\left([O]_{fn}+[P]_{fn}\right)};FB_{fp}=\frac{[O]_{fp}-[P]_{fp}}{0.5\left([O]_{fp}+[P]_{fp}\right)} \tag{8}$$

Normalized mean square error (*NMSE*):

$$NMSE=\frac{[(O-P)^2]}{[O][P]} \tag{9}$$

In these definitions, O_i and P_i correspond to the observed (measured) and predicted (computed) values of a given variable for the sample i, respectively; N is the number of data points; D_q and W_q are the allowed relative and absolute deviations, respectively. The square brackets denote averaging on the whole dataset or on all the under- (resp. over-) predictions when they are followed by the subscript *fn* (resp. *fp*). Note that *FB* and *NMSE* cannot be used for variables that can take both positive and negative values and have therefore been used only for k.

The values of the relative and absolute error thresholds for q have been taken equal to D_q=0.25 and W_q=0.03 for velocity and to D_q=0.25 and W_q=0.003 for k. The threshold for absolute error is based on the uncertainty of the experiment. Here, the uncertainty on velocity measurements was not explicitly mentioned in the experimental report but it was estimated based on the anemometer manufacturer information (Jørgensen, 2002) and experiments performed with the same equipment (Ubertini and Desideri, 2000).

4. Validation: comparison with the measurements

4.1. Influence of the inlet method

The profiles of mean streamwise velocity along 5 lines (x/b=-0.75; -0.25; 0.5; 1.25; 3.25) in the planes V0 and H10 obtained for LES20-1 and LES20-5 are compared to the measurements in Fig. 3. The agreement with the experiment is very good for LES20-1, in both planes. The recirculation zones over the roof and in the wake of the building, where U<0, are well described: the computed roof (X_r) and wake (X_w) recirculation lengths compare well with the measurements (Table 4). Note that the LES simulation by Tominaga et al. (2008a) – for which the results are also shown in Table 4 – uses a precursor simulation to generate the turbulent inflow. With a steady inlet (LES20-5), discrepancies in the velocity profiles appear around roof level and in the far wake, which is confirmed by the metric values shown in Table 3. LES20-5 shows a stronger over-estimation of X_r and X_w (Table 4), in agreement with Yoshie et al. (2011) who performed LES of flow around a building with the same geometry as the one considered here, with and without inflow turbulence.

The main difference between the two simulations is found for the turbulent kinetic energy field (Fig. 4). The k-values computed by LES20-5 upstream of the building are close to zero, because of the absence of velocity fluctuations at the inlet. The building generates turbulence in its vicinity but k remains largely under-estimated by LES20-5 on all the measurement lines (hit-rate value: q=0.17). This result is in contradiction with Tominaga et al. (2008a) who found higher k behind the building in the absence of

inflow turbulence because of the more intense vortex shedding. Here, when the VM is used to generate inflow turbulence (LES20-1), a rather good agreement is found between CFD and experiment (q=0.65).

It is verified a posteriori that the time-averaged inlet profiles generated by the VM correspond eventually to the experimental/prescribed profiles. The inlet profiles of U/U_h and k/U_h^2 averaged along the y-direction for LES20-1 and LES30-1 are shown in Fig. 5. In both cases, the resulting profile of U is identical to what has been prescribed (Fig. 5a). The resulting inlet profile of k (computed based on the velocity fluctuations at every time step of the averaging period of the simulation) is slightly different for LES20-1 and LES30-1, showing that the VM is a grid-dependent technique (Fig. 5b). This should be kept in mind when comparing the results of these two simulations. The symmetry boundary conditions used on the sides of the domain limit the fluctuations of the lateral velocity at these locations, resulting in a decrease of k. This explains the slight under-estimation of the y-averaged k-profiles compared to the prescribed values. If the vertical centerline of the inlet plane is considered, a good agreement is found between the prescribed and resulting k-profiles (not shown here). A closer look at the individual normal stresses reveals however that the VM under-estimates σ_u on this line (by about 30% and 10% at building height for LES 20-1 and LES30-1, respectively), which is compensated by the over-estimation of σ_w. The standard deviation of the lateral velocity component (σ_v) computed by the VM is in good agreement with the measurements.

4.2. Influence of the SGS model

The influence of the SGS model is presented here for Grid20. As can be seen in Figure 6, the mean streamwise velocity profiles obtained with the Smagorinsky SGS model and C_s=0.1 (LES20-1), with the dynamic Smagorinsky SGS model (LES20-3), and without SGS model (LES20-4) are very close to each other and in very good agreement with the measurements (q=0.89-0.90). With C_s=0.15 (LES20-2), U is slightly over-estimated in the plane H10 but the agreement remains good, with an overall hit-rate value of 0.87. The recirculation lengths predicted by the three simulations are very close to each other and slightly over-estimate the measured ones (Table 4).

Like for U/U_h, the k-values computed with LES20-1, LES20-3 and LES20-4 are very similar (Fig. 7). LES20-2 over-estimates k in comparison with experimental results – especially in the wake of the building – and provides higher values than LES20-1. This lower performance of the Smagorinsky model with C_s=0.15 is also seen in the validation metrics in Table 3 and supports the appropriateness of C_s=0.1 to simulate the flow around this isolated bluff body. Note that the difference between the different SGS models is smaller on Grid30 (not shown here).

Several earlier studies have applied implicit LES (i.e. without explicit model for the subgrid scales) to flow around buildings (e.g. Patnaik et al., 2007; Köse and Dick, 2010). Köse and Dick (2010) have studied the pressure distribution on a cubical building immerged in a channel flow and in an ABL flow. They have used the bounded central-differencing scheme (the one used here) to discretize the convective terms of the transport equations and shown the suitability of this scheme to implicit LES: the truncation error introduced when discretizing the equations acts implicitly as an SGS model. This is the reason why good agreement with experimental data is observed in the present study for LES20-4. Note that this holds also for the fine grid (LES30-4), as can be seen in Tables 3 and 4.

4.3. Influence of the grid resolution

With LES and implicit filtering, the model depends inherently on the grid size. When refining the grid, the model contribution is also changing and consequently a grid-independent solution cannot be found (Freitag and Klein, 2006). Nevertheless, LES20-1 and LES30-1 are compared here to investigate the influence of the grid resolution on the results. Both computations use the standard Smagorinsky SGS model with C_s=0.1. No major changes in the computed values of U/U_h are implied by the use of the fine grid, as can be seen in Fig. 8 and from the validation metrics values (Table 3). The low dependence of the

mean velocity results on the grid resolution was also observed with C_s=0.15 and with the dynamic Smagorinsky SGS model (not shown here).

The smaller the grid size, the larger is the range of eddy scales which are resolved by the LES model. As a consequence, the contribution of a larger range of scales to the velocity fluctuations is taken into account by the simulations on Grid30, and the resolved turbulent kinetic energy with this grid is higher than with Grid20. These considerations are eventually observed in our results but in this particular case the agreement with the measurements deteriorates (Fig. 9). The conclusion is therefore rather counter-intuitive: the coarsest mesh is the one which provides the best agreement with the measurements. A discussion on this issue can be found in (Celik et al., 2005), giving the under-estimation of the turbulence dissipation rate as a possible explanation for the over-estimation of k by LES on the fine grid. Similar results can also be found in (Meyers et al., 2003) and (Klein, 2005). In the former reference, the authors show that the modeling and numerical error on the computation of k counteract. Hence, although the two error components are higher in magnitude on a coarse grid than on a finer one, the sum (total error) is higher on the fine grid. Bias error in the measurements of the velocity fluctuations is another possible explanation for the discrepancy between CFD and experiment in terms of k, as well as the difference between the sampling frequency used in the measurements and the one used in the CFD simulations.

5. Solution verification

5.1. Monitoring of statistical convergence

Fig. 10a shows the evolution of the non-dimensional moving-average of the streamwise velocity $<u>_t/U_h$ as a function of time in the averaging period ($0 \le t \le T_{avg}$) at four monitoring points located in different zones of the flow-field (see Fig. 10b). These results correspond to the simulation on the coarse grid with the dynamic Smagorinsky SGS model (LES20-3). It appears that the variations of $<u>_t$ are relatively low at the end of the averaging period (16,000 time steps in this case). The convergence of the mean value is quantified by $e_{conv}(\%)$, defined for a given range of time steps I by:

$$e_{conv}(I) = 100 \times \left| \frac{\max_{k \in I}(< u >_{k\Delta t}) - \min_{k \in I}(< u >_{k\Delta t})}{< u >_{T_{avg}}} \right| \qquad (10)$$

This indicator corresponds to the range of values that the moving-average takes within an interval I of time steps numbers in the averaging period (for example I=1,…,2000), normalized by the final average value at $t=T_{avg}$. The 16,000 time steps of the averaging period of LES20-3 have been divided into eight equal intervals for which the values of e_{conv} are reported in Table 5 for P1, P2, P3 and P4. At the beginning of the averaging period (time steps 1 to 2000) each instantaneous flow pattern has a high influence on $<u>_t$ and the values of e_{conv} are therefore high at every point, especially at P2 and P3. e_{conv} shows a decreasing trend and reaches low values (≤4.1%) at the end of the averaging period, which indicates sufficient statistical convergence of the simulation. Note that the points P2 and P3 are located in regions of the flowfield where quasi-periodic flow patterns occur (Wang and Zhou, 2009) and limit the convergence of the statistics. Observing the evolution of e_{conv} at these points is therefore a conservative way to assess the statistical convergence of the simulation.

5.2. Systematic Grid and Model Variation (SGMV)

When the filter width and the grid spacing are independent (explicit filtering), the modeling (ε_m) and numerical (ε_n) errors can be estimated separately: the "grid-independent" LES solution – which does exist for a given filter width in the context of explicit filtering – is compared on the one hand to the filtered

DNS solution to provide an estimation of ε_m, and on the other hand to the LES solution on a coarse grid (at constant filter width) to provide an estimation of ε_n (Vreman et al., 1996; Geurts and Fröhlich, 2002; Meyers et al., 2003). By contrast, in the context of implicit filtering, as already mentioned, the modeling and numerical errors interact and cannot be evaluated separately. The SGMV (Klein, 2005) is therefore used here to provide an estimation of these two types of error, based on Richardson extrapolation. The difference between the exact solution of the flow equations (u_e) and the numerical solution on a given grid (say $u_{20\text{-}1}$ for LES20-1) is equal to the sum of these two error contributions which are assumed to scale with the filter width:

$$u_e - u_{20-1} = \varepsilon_m^{20-1} + \varepsilon_n^{20-1} = c_m \Delta_{20}^m + c_n \Delta_{20}^n \tag{11}$$

where n is the order of accuracy of the numerical scheme (taken here equal to 2 (Manickam et al., 2012)), m is set to its theoretical value 2/3 as suggested in (Freitag and Klein, 2006), c_m and c_n are coefficients to be determined. Following the same approach for LES20-2 and LES30-1 yields:

$$u_e - u_{20-2} = \varepsilon_m^{20-2} + \varepsilon_n^{20-2} = \beta c_m \Delta_{20}^m + c_n \Delta_{20}^n \tag{12}$$

$$u_e - u_{30-1} = \varepsilon_m^{30-1} + \varepsilon_n^{30-1} = c_m (\Delta_{20} / \alpha)^m + c_n (\Delta_{20} / \alpha)^n \tag{13}$$

where $\beta = C_s^2{}_{|20\text{-}2} / C_s^2{}_{|20\text{-}1} = 2.25$ is the model variation factor and α is the grid coarsening factor defined earlier. Hence, the combination of the numerical solutions of these three simulations allows determining the unknowns of the problem (u_e, c_m and c_n) and estimating the numerical and SGS modeling errors. The SGMV technique has been applied here for the mean velocity. The procedure has been repeated on LES30-1, LES30-2 and LES20-1 to evaluate the numerical and modeling errors for LES30-1.

Figs. 11 and 12 show the resulting estimation of ε_m and ε_n normalized by U_h for LES20-1 and LES30-1, respectively. The sum of these two error contributions is also shown. Note that it is advised to use the sum of the magnitudes $|\varepsilon_m|+|\varepsilon_n|$ as a conservative estimate of the total error (Freitag and Klein, 2006). The numerical error is relatively high for LES20-1, especially above roof level and in the wake of the building (Fig. 11a) as well as in the side shear layer (Fig. 11b) where it can reach up to 15% of the reference velocity. Noticeably, the SGS modeling error is generally of opposite sign than the one of ε_n, with similar order of magnitude, which significantly decreases the total error on mean velocity (see (Vreman et al., 1996) and (Meyers et al., 2003) for similar results in the case of mixing layer and homogeneous isotropic turbulence, respectively). Concerning LES30-1, a similar trend is observed for the numerical error but its magnitude is lower than on the coarse grid (Fig. 12). As mentioned earlier, the SGS model had low influence on the mean velocity with Grid30; it is confirmed here by the very low estimated values of ε_m. Despite the higher magnitude of errors on LES20-1, the compensation that operates between ε_m and ε_n leads to a similar level of total error in this case in comparison with LES30-1, which explains why similar results were obtained for the mean velocity field on the two grids. The conservative estimate of the total error $|\varepsilon_m|+|\varepsilon_n|$, however, is clearly higher on the coarse mesh.

5.3. LES Index of Quality

Since a grid-independent solution cannot be achieved with LES and implicit filtering, a way to determine whether a given grid is suitable is to evaluate the amount of turbulent kinetic energy that it allows resolving. This is the purpose of the LES index of quality (*LES_IQ*) (Celik et al., 2005). The total kinetic energy (k_{tot}) can be decomposed into the resolved part (k), the contribution of the SGS model (k_{SGS}), and the contribution of the numerical dissipation (k_{num}).

$$LES\_IQ = \frac{k}{k_{tot}} = \frac{k}{k + k_{SGS} + k_{num}} = 1 - \frac{k_{tot} - k}{k_{tot}} \tag{14}$$

As suggested by Pope (2000), an LES computation can be judged to be well-resolved when 80% of the turbulent kinetic energy is resolved. In some cases, k is found to be higher on a coarser grid than on a finer one, especially in regions near walls. The reason for this anomaly is not totally clear, according to Celik et al. (2005). This was observed in the present computations (above roof level and in regions of very low k) so the generalized formula has been used to keep *LES_IQ* below the ideal value of 1, as advised in the aforementioned article:

$$LES\_IQ = 1 - \frac{|k_{tot} - k|}{k_{tot}} \tag{15}$$

Based on Richardson extrapolation, the combined contribution of SGS model and numerical diffusion is assumed to scale with the grid size/filter length (Celik et al., 2005):

$$k_{tot} - k = a_k \Delta^n \tag{16}$$

where n=2 is the order of accuracy of the numerical scheme and a_k is a coefficient that can be determined by running the simulation on two grids with different resolution (cases LES20-1 and LES30-1 here).

Fig. 13 shows the profiles of *LES_IQ* along the same lines that were used in the validation part, as well as the averaged values of *LES_IQ* on each line for $z/b<3$ (plane V0) and $-3<y/b<0$ (plane H10). As expected, the simulation on Grid30 resolves a larger part of the total turbulent kinetic energy. On the nine measurement lines in the plane V0 for $z/b<3$, on average 89% of k_{tot} is resolved by LES30-1 compared to 76% by LES20-1 (Fig. 13a). The flow regions where the least energy is resolved are the upstream part of the roof ($-0.5<x/b<0$) and the far-wake ($x/b\approx3.25$). Keeping the grid uniform in these regions instead of imposing a cell growth would help increasing the amount of resolved energy. On the measurement lines in H1 and H10, for $-3<y/b<0$, LES30-1 resolves on average 91% and 93% of k_{tot}, respectively, while LES20-1 resolves 80% and 84%. The profiles of *LES_IQ* in the plane H10 are shown in Fig. 13b. On average over all the measurement lines, LES20-1 and LES30-1 resolve 80% and 91% of k_{tot}, respectively. Thus, if the threshold of 80% is used to define a well-resolved LES, both simulations can be classified in this category. Noticeably, while LES30-1 resolves a larger proportion of the turbulent kinetic energy, Section 4 has also shown that this simulation over-estimates the experimental values.

6. Summary and conclusions

Large-Eddy Simulation of wind flow around a high-rise building has been performed with the commercial CFD code Ansys/Fluent 12.1. Several cases have been run and analyzed, on two different grids (Grid20 and Grid30) and with two different SGS models, namely the standard Smagorinsky model and its dynamic version. For the former, C_s=0.1 and 0.15 have been tested. The results have been compared with wind-tunnel measurements in terms of non-dimensional mean velocity U/U_h and turbulent kinetic energy k/U_h^2. The agreement between numerical and experimental results has been quantified by validation metrics (hit rate, FAC2, FB and NMSE). A posteriori solution verification has been performed with Systematic Grid and Model Variation (SGMV) and the *LES_IQ* indicator. These techniques have been developed for general fluid engineering problems and, to the best of the authors' knowledge, have been applied here for the first time to LES of wind flow around a building. From this study, the following conclusions can be drawn:

- The vortex method to generate time-dependent velocity profile at the inlet of the domain has been shown to be suitable for atmospheric boundary layer flows.
- A suitable length for the averaging period has been determined by monitoring the moving average of velocity at several points in the flow field: 718 time units or 21.8 flow-through times.
- Very good agreement was found for all cases for the mean streamwise velocity field (hit rate values between 0.84 and 0.90). The other components and the velocity fluctuations appeared to be more challenging to predict (e.g. hit rate values below 0.66 for k).
- With the standard Smagorinsky SGS model, the use of C_s=0.1 provided the most accurate results, very close to those of the dynamic Smagorinsky model.
- Good accuracy was also found without explicit SGS model, showing that the numerical error introduced with the bounded central-differencing scheme acts implicitly as an SGS model.
- Unexpectedly, the best agreement between numerical and experimental values of k was found on the coarse grid. Note however that similar results were found by other authors in the past.
- The SGMV technique showed that the SGS modeling and numerical errors were rather high for the simulation on Grid20. However, both error contributions are of opposite sign and eventually compensate each other, leading to a total error comparable to the one on the fine grid and explaining the similarity of the computed values of U on the two grids.
- The estimation of the modeling error for U by SGMV showed that it was very low for C_s=0.1 on Grid30, which is linked to the small difference in mean velocity results obtained on the fine grid with different C_s values (no plots were shown here).
- According to the *LES_IQ* indicator, the simulations with the standard Smagorinsky model and C_s=0.1 with 20 (LES20-1) and 30 cells (LES30-1) per building side can be both classified as well-resolved LESs in the sense that they resolve at least 80% of the total turbulent kinetic energy in the region around the building (LES20-1: 80% on average; LES30-1: 91%)
- The over-estimation of the measured values of k by LES30-1 was observed. The reason for this is not totally clear and this result needs to be confirmed on another test case.

Future research on this topic will consist of:
- Applying the SGMV procedure to the turbulent kinetic energy, on the same validation case.
- Repeating the complete procedure on another validation experiment of flow around bluff bodies, for confirmation.
- Testing the influence of the time step size. In particular, the spectra of velocity fluctuations should be analyzed to further explain the k-values computed by LES.
- Repeating the study with another CFD code (e.g. OpenFOAM).
- Applying the procedure to other configurations representative of the built environment. Guidelines on the use of LES in wind engineering could be deduced from the presented results.

Acknowledgements.

The authors thank Dr. Jörg Franke for his valuable comments on the manuscript. The authors also thank the anonymous reviewers for their valuable comments on the manuscript.

7102 words.

References

Initiative on "Harmonisation within Atmospheric Dispersion Modelling for Regulatory Purposes", http://www.harmo.org/, 2012.

AIAA. 1998. Guide for the verification and validation of Computational Fluid Dynamics simulations AIAA-G-077-1998.

Ansys Inc., 2009. Ansys Fluent 12.0 - Theory Guide, Lebanon, USA.

Bell, J.B., Colella, P., Glaz, H.M., 1989. A second-order projection method for the incompressible Navier-Stokes equations. Journal of Computational Physics 85, 257-283.

Blocken, B., Carmeliet, J., Stathopoulos, T., 2007a. CFD evaluation of wind speed conditions in passages between parallel buildings–effect of wall-function roughness modifications for the atmospheric boundary layer flow. Journal of Wind Engineering and Industrial Aerodynamics 95, 941-962.

Blocken, B., Stathopoulos, T., Carmeliet, J., 2007b. CFD simulation of the atmospheric boundary layer: wall function problems. Atmospheric Environment 41, 238-252.

Blocken, B., Janssen, W.D., van Hooff, T., 2012. CFD simulation for pedestrian wind comfort and wind safety in urban areas: General decision framework and case study for the Eindhoven University campus. Environmental Modelling & Software 30, 15-34.

Casey, M., Wintergerste, T. (Eds.), 2000. Best Practice Guidelines; ERCOFTAC Special Interest Group on "Quality and Trust in Industrial CFD". Version 1.0, 94pp.

Celik, I., Cehreli, Z.N., Yavuz, I., 2005. Index of resolution quality for Large Eddy Simulation. Journal of Fluids Engineering 127, 949-958.

Celik, I., Klein, M., Freitag, M., Janicka, J., 2006. Assessment measures for URANS/DES/LES: an overview with applications. Journal of Turbulence 7, 1-27.

Celik, I., Klein, M., Janicka, J., 2009. Assessment measures for engineering LES applications. Journal of Fluids Engineering 131, 10 pages.

Franke, J., Hellsten, A., Schlünzen, H., Carissimo, B. (Eds.); 2007. Best practice guideline for the CFD simulation of flows in the urban environment, COST Action 732.

Franke, J. 2010. A review of verification and validation in relation to CWE. The Fifth International Symposium on Computational Wind Engineering, Chapel Hill, North Carolina, USA.

Freitag, M., Klein, M., 2006. An improved method to assess the quality of large eddy simulations in the context of implicit filtering. Journal of Turbulence 7, 1-11.

Gaskell, P.H., Lau, A.K.C., 1988. Curvative-compensated convective transport: SMART, a new boundedness-preserving transport algorithm. International Journal for Numerical Methods in Fluids 8, 617-641.

Germano, M., Piomelli, U., Moin, P., Cabot, W.H., 1991. A dynamic subgrid-scale eddy viscosity model. Physics of Fluids A 3, 1760-1765.

Geurts, B.J., Fröhlich, J., 2002. A framework for predicting accuracy limitations in large-eddy simulation. Physics of Fluids 14, 41-L44.

Ghosal, S., Moin, P., 1995. The basic equations for the Large Eddy Simulation of turbulent flows in complex geometry. Journal of Computational Physics 118, 24-37.

Gousseau, P., Blocken, B., Stathopoulos, T., van Heijst, G.J.F., 2011a. CFD simulation of near-field pollutant dispersion on a high-resolution grid: a case study by LES and RANS for a building group in downtown Montreal. Atmospheric Environment 45, 428-438.

Gousseau, P., Blocken, B., van Heijst, G.J.F., 2011b. CFD simulation of pollutant dispersion around isolated buildings: On the role of convective and turbulent mass fluxes in the prediction accuracy. Journal of Hazardous Materials 194, 422-434.

Gousseau, P., Blocken, B., van Heijst, G.J.F., 2012. Large-Eddy Simulation of pollutant dispersion around a cubical building: Analysis of the turbulent mass transport mechanism by unsteady concentration and velocity statistics. Environmental Pollution 167, 47-57.

Hanna, S.R., Brown, M.J., Camelli, F.E., Chan, S.T., Coirier, W.J., Hansen, O.R., Huber, A.H., Kim, S., Reynolds, R.M., 2006. Detailed simulations of atmospheric flow and dispersion in downtown

Manhattan. An application of five computational fluid dynamics models. Bulletin of the American Meteorological Society 87, 1713-1726.
Jørgensen, F.E., 2002. How to measure turbulence with hot-wire anemometers - A practical guide, Dantec Dynamics.
Kim, J., Moin, P., 1985. Application of a fractional step method to incompressible Navier-Stokes equations. Journal of Computational Physics 59, 308-323.
Klein, M., 2005. An attempt to assess the quality of large eddy simulations in the context of implicit filtering. Flow, Turbulence and Combustion 75, 131-147.
Klein, M., Meyers, J., Geurts, B.J. 2008. Assessment of LES quality measures using the error landscape approach. Quality and reliability of Large-Eddy Simulations, Springer.
Köse, D.A., Dick, E., 2010. Prediction of the pressure distribution on a cubical building with implicit LES. Journal of Wind Engineering and Industrial Aerodynamics 98, 628-649.
Lilly, D.K., 1992. A proposed modification of the Germano subgrid-scale closure method. Physics of Fluids A 4, 633-635.
Lim, H.C., Thomas, T.G., Castro, I.P., 2009. Flow around a cube in a turbulent boundary layer: LES and experiment. Journal of Wind Engineering and Industrial Aerodynamics 97, 96-109.
Manickam, B., Franke, J., Muppala, S., Dinkelacker, F. 2012. Large-eddy Simulation of Triangular-stabilized Lean Premixed Turbulent Flames: Quality and Error Assessment. Flow, Turbulence and Combustion 88, 563-596.
Mathey, F., Cokljat, D., Bertoglio, J.P., Sergent, E., 2006. Assessment of the vortex method for large eddy simulation inlet conditions. Progress in Computational Fluid Dynamics 6, 58-67.
Meng, Y., Hibi, K., 1998. Turbulent measurements of the flow field around a high-rise building. Journal of Wind Engineering 76, 55-64.
Meyers, J., Geurts, B.J., Baelmans, M., 2003. Database analysis of errors in large-eddy simulation. Physics of Fluids 15, 2740-2755.
Moin, P., Reynolds, W.C., Ferziger, J.H., 1978. Large Eddy Simulation of incompressible turbulent channel flow. Stanford University, Dpt. of Mechanical Engineering. Report TF-12, 134 pp.
Murakami, S., 1993. Comparison of various turbulence models applied to a bluff body. Journal of Wind Engineering and Industrial Aerodynamics 46 & 47, 21-36.
Nozu, T., Tamura, T., Okuda, Y., Sanada, S., 2008. LES of the flow and building wall pressures in the center of Tokyo. Journal of Wind Engineering and Industrial Aerodynamics 96, 1762-1773.
Oberkampf, W.L., Trucano, T.G., 2002. Verification and validation in computational fluid dynamics. Progress in Aerospace Sciences 38, 209-272.
Patnaik, G., Boris, J.P., Young, T.R., Grinstein, F.F., 2007. Large scale urban contaminant transport simulations with Miles. Journal of Fluids Engineering 129, 1524-1532.
Pope, S.B., 2000. Turbulent flows, Cambridge University Press, 806 pp.
Ramponi, R., Blocken, B., 2012. CFD simulation of cross-ventilation for a generic isolated building: Impact of computational parameters. Building and Environment 53, 34-48.
Roache, P.J., 1998. Verification and validation in computational science and engineering, Hermosa Publisher, Albuquerque, NM, 446 pp.
Rodi, W., 1997. Comparison of LES and RANS calculations of the flow around bluff bodies. Journal of Wind Engineering and Industrial Aerodynamics 69-71, 55-75.
Rodi, W., Ferziger, J.H., Breuer, M., Pourquié, M., 1997. Status of Large Eddy Simulation: Results of a workshop. Journal of Fluid Engineering 119, 248-262.
Schatzmann, M., Olesen, H., Franke, J., 2010. COST 732 model evaluation case studies: approach and results, COST Action 732, .
Sergent, E. 2002. Vers une méthode de couplage entre la simulation des grandes échelles et les modèles statistiques. PhD thesis, Ecole doctorale MEGA, Ecole Centrale de Lyon.
Shah, K.B., Ferziger, J.B., 1997. A fluid mechanicians view of wind engineering: Large eddy simulation of flow past a cubic obstacle. Journal of Wind Engineering and Industrial Aerodynamics 67-68, 211-224.

Smagorinsky, J., 1963. General circulation experiments with the primitive equations. I. The basic experiment. Monthly Weather Review 91, 99-164.
Srebric, J., Chen, Q., 2002. An example of verification, validation, and reporting of indoor environment CFD analyses. ASHRAE Transactions 108(2), 185-194.
Tamura, T., 2008. Towards practical use of LES in wind engineering. Journal of Wind Engineering and Industrial Aerodynamics 96, 1451-1471.
Thomas, T.G., Williams, J.J.R., 1997. Development of a parallel code to simulate skewed flow over a bluff body. Journal of Wind Engineering and Industrial Aerodynamics 67 & 68, 155-167.
Tominaga, Y., Mochida, A., Murakami, S., Sawaki, S., 2008a. Comparison of various revised k-ε models and LES applied to flow around a high-rise building model with 1:1:2 shape placed within the surface boundary layer. Journal of Wind Engineering and Industrial Aerodynamics 96, 389-411.
Tominaga, Y., Mochida, A., Yoshie, R., Kataoka, H., Nozu, T., Yoshikawa, M., Shirasawa, T., 2008b. AIJ guidelines for practical applications of CFD to pedestrian wind environment around buildings. Journal of Wind Engineering and Industrial Aerodynamics 96, 1749-1761.
Tominaga, Y., Stathopoulos, T., 2010. Numerical simulation of dispersion around an isolated cubic building: model evaluation of RANS and LES. Building and Environment 45 (10), 2231-2239.
Tominaga, Y., Stathopoulos, T., 2011. CFD modeling of pollution dispersion in a street canyon: Comparison between LES and RANS. Journal of Wind Engineering and Industrial Aerodynamics 99, 340-348.
Tseng, Y.H., Meneveau, C., Parlange, M.B., 2006. Modeling flow around bluff bodies and predicting urban dispersion using large eddy simulation. Environmental Science & Technology 40, 2653-2662.
Ubertini, S., Desideri, U., 2000. Flow development and turbulence length scales within an annular gas turbine exhaust diffuser. Experimental Thermal and Fluid Science 22, 55-70.
van Hooff, T., Blocken, B., 2010. Coupled urban wind flow and indoor natural ventilation modelling on a high-resolution grid: A case study for the Amsterdam ArenA stadium. Environmental Modelling & Software 25, 51-65.
van Hooff, T., Blocken, B., Aanen, L., Bronsema, B., 2011. A venturi-shaped roof for wind-induced natural ventilation of buildings: wind tunnel and CFD evaluation of different design configurations. Building and Environment 46(9): 1797-1807.
Vasilyev, O.V., Lund, T.S., Moin, P., 1998. A general class of commutative filters for LES in complex geometries. Journal of Computational Physics 146, 82-104.
Vreman, A.W., Geurts, B.J., Kuerten, J.G.M., 1996. Comparison of numerical schemes in large eddy simulation of the temporal mixing layer. International Journal for Numerical Methods in Fluids 22, 299-311.
Wang, H.F., Zhou, Y., 2009. The finite-length square cylinder near wake. Journal of Fluid Mechanics 638, 453-490.
Xie, Z.T., Castro, I.P., 2009. Large-eddy simulation for flow and dispersion in urban streets. Atmospheric Environment 43, 2174-2185.
Yoshie, R., Mochida, A., Tominaga, Y., Kataoka, H., Harimoto, K., Nozu, T., Shirasawa, T., 2007. Cooperative project for CFD prediction of pedestrian wind environment in the Architectural Institute of Japan. Journal of Wind Engineering and Industrial Aerodynamics 95, 1551-1578.
Yoshie, R., Jiang, G., Shirasawa, T., Chung, J., 2011. CFD simulations of gas dispersion around high-rise building in non-isothermal boundary layer. Journal of Wind Engineering and Industrial Aerodynamics 99, 279-288.

Figure captions

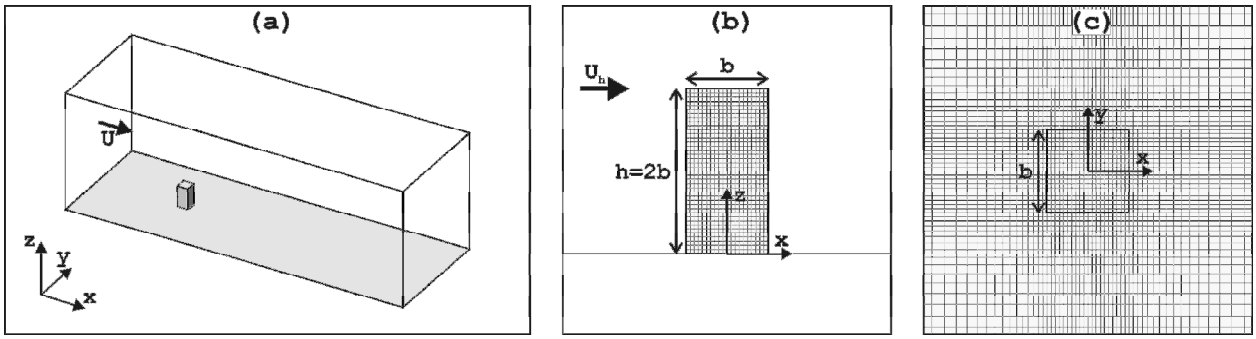

Figure 1. (a) Computational domain. (b) Side and (c) top view of the grid on the building and ground surfaces for Grid20 (total number of cells: 737,920).

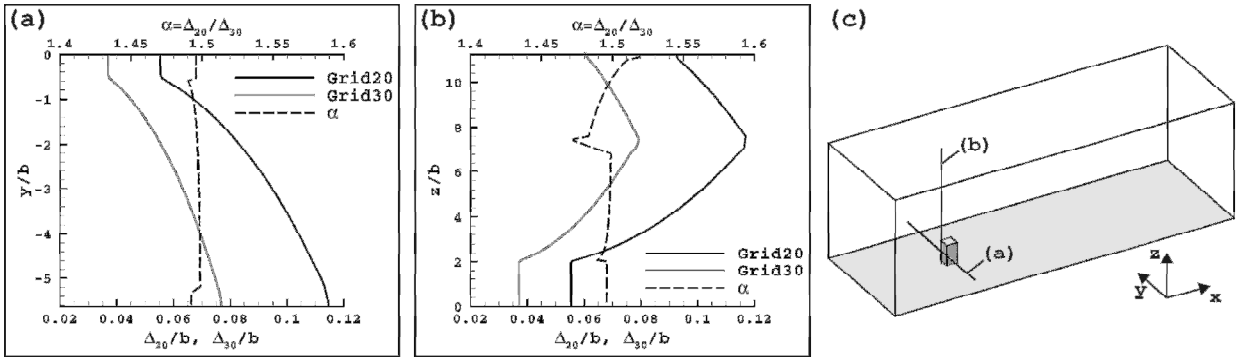

Figure 2. Profiles of non-dimensional filter width Δ_{20}/b and Δ_{30}/b along the lines (a) (x/b=-0.75; z/b=1.25) and (b) (x/b=-0.75; y/b=0) for the two computational grids used in this study. The grid coarsening factor α is also shown (dashed line and secondary axis). (c) shows the position of the plotting lines.

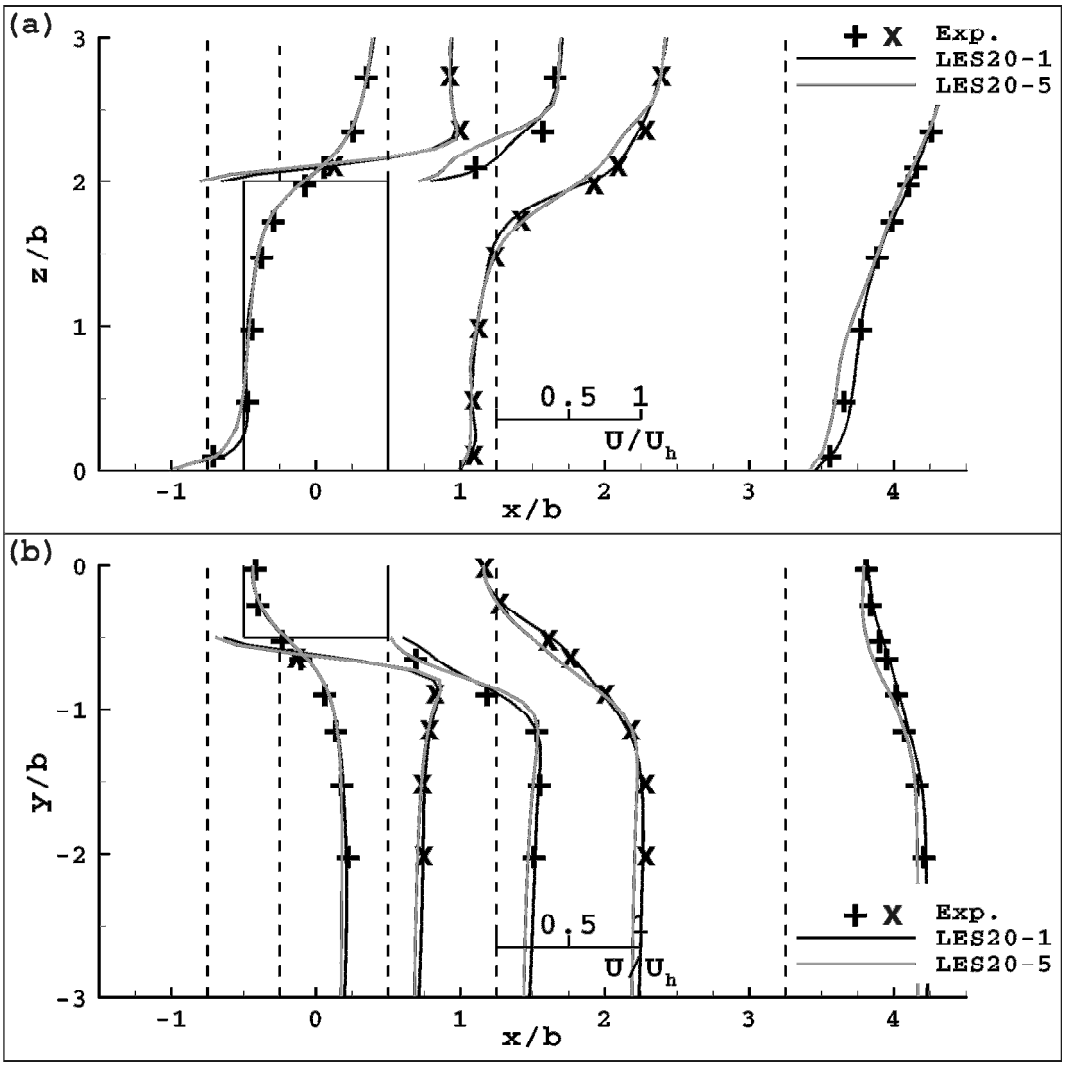

Figure 3. Validation of the Vortex Method (VM): comparison between LES20-1 (VM) and LES20-5 (no perturbation at inlet). Experimental (symbols) and numerical (lines) profiles of non-dimensional mean streamwise velocity in the planes (a) V0 and (b) H10.

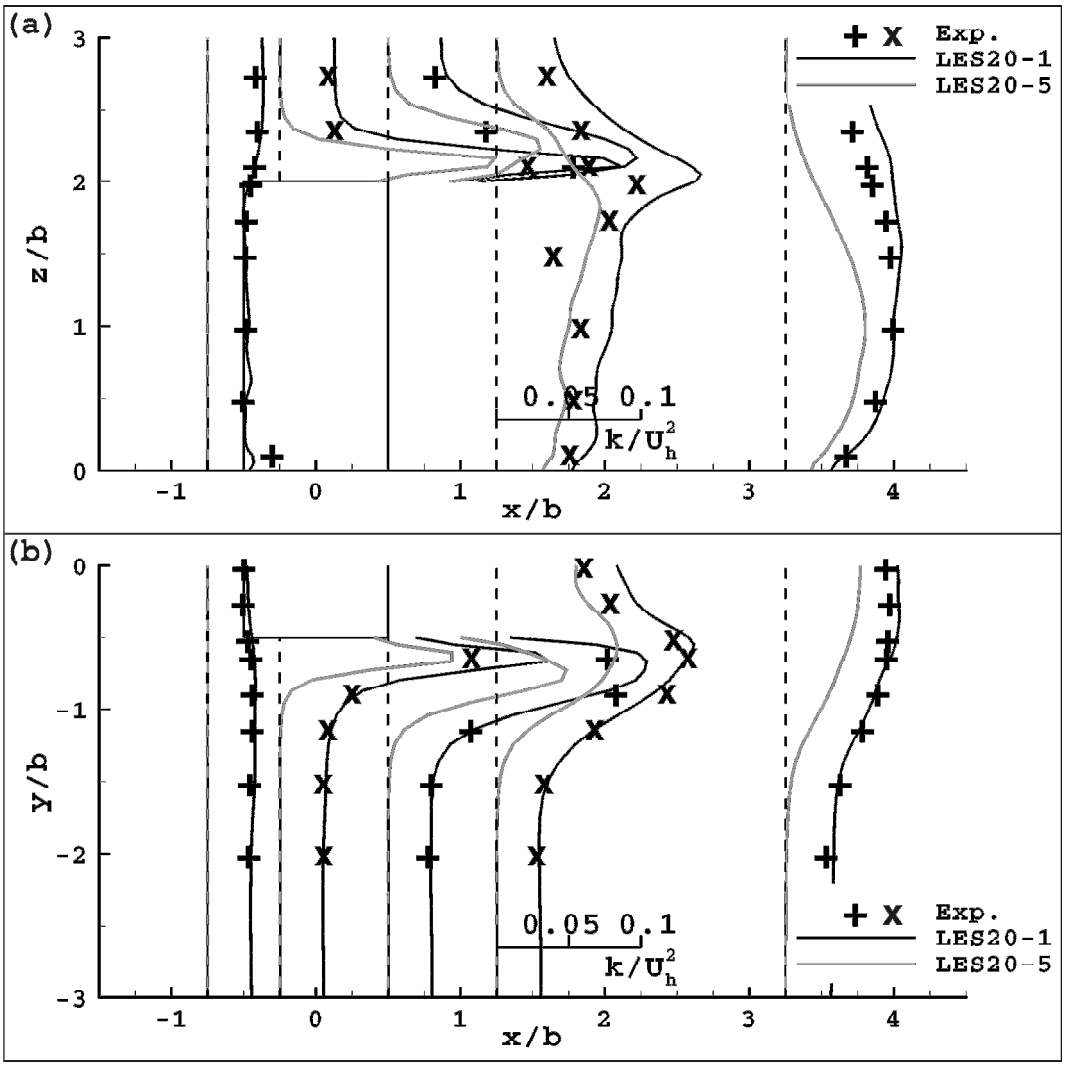

Figure 4. Validation of the vortex method (VM): comparison between LES20-1 (VM) and LES20-5 (no perturbation at inlet). Experimental (symbols) and numerical (lines) profiles of non-dimensional turbulent kinetic energy in the planes (a) V0 and (b) H10.

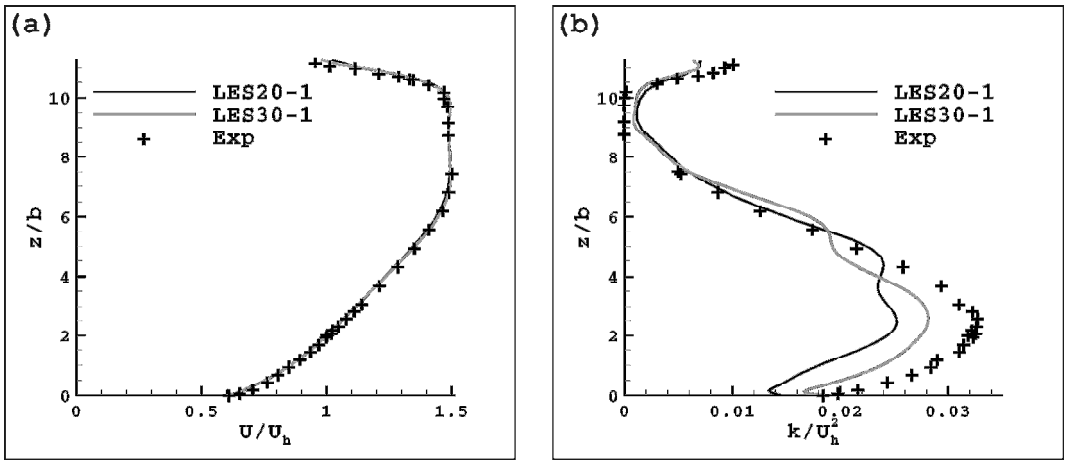

Figure 5. Experimental/prescribed profiles (symbols) and resulting time-average profiles at the inlet for LES20-1 and LES30-1 (lines) of (a) non-dimensional streamwise velocity and (b) non-dimensional turbulent kinetic. The numerical results are averaged in the lateral direction.

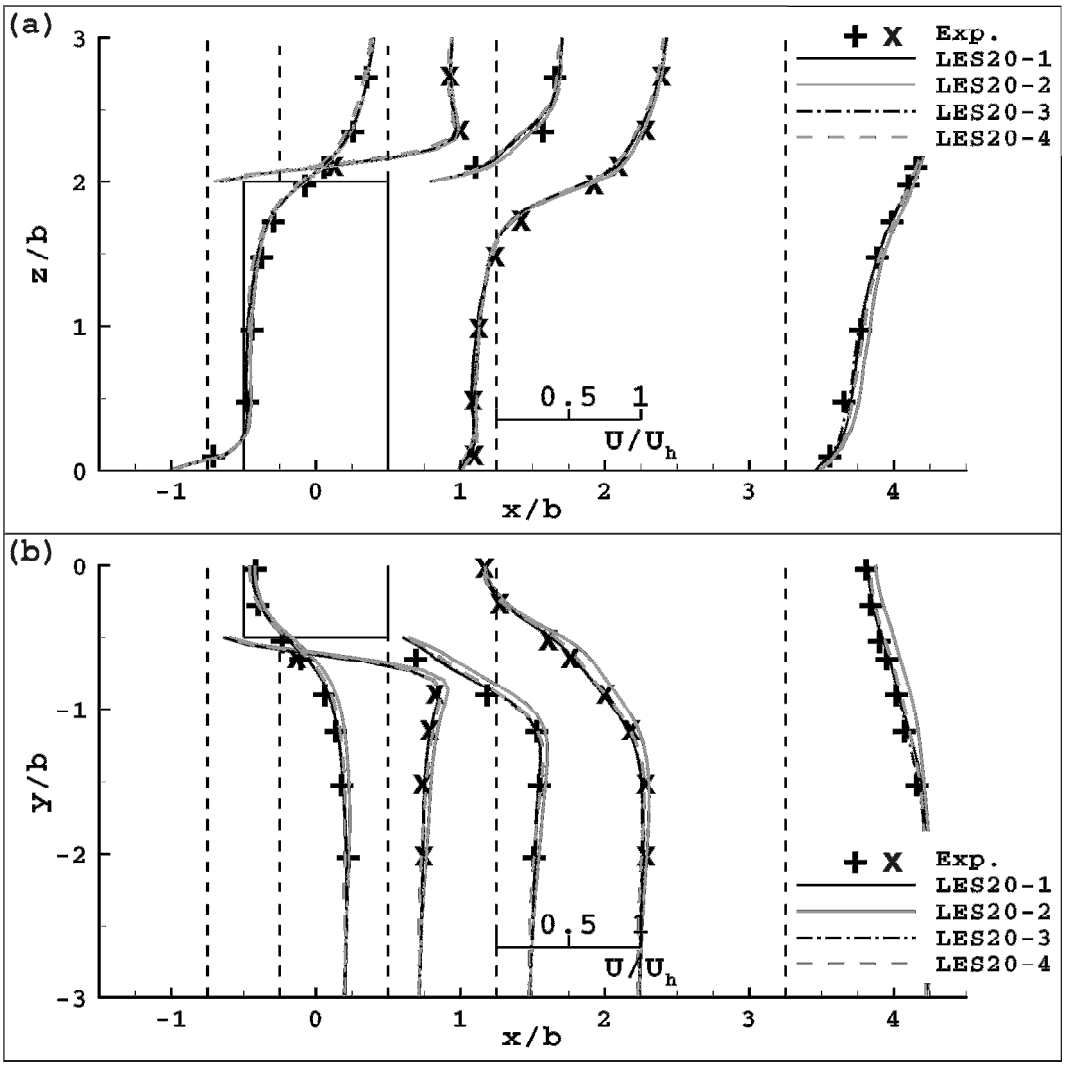

Figure 6. Influence of the SGS model: comparison between LES20-1 (C_s=0.1), LES20-2 (C_s=0.15), LES20-3 (dynamic) and LES20-4 (no SGS model). Experimental (symbols) and numerical (lines) profiles of non-dimensional mean streamwise velocity in the planes (a) V0 and (b) H10.

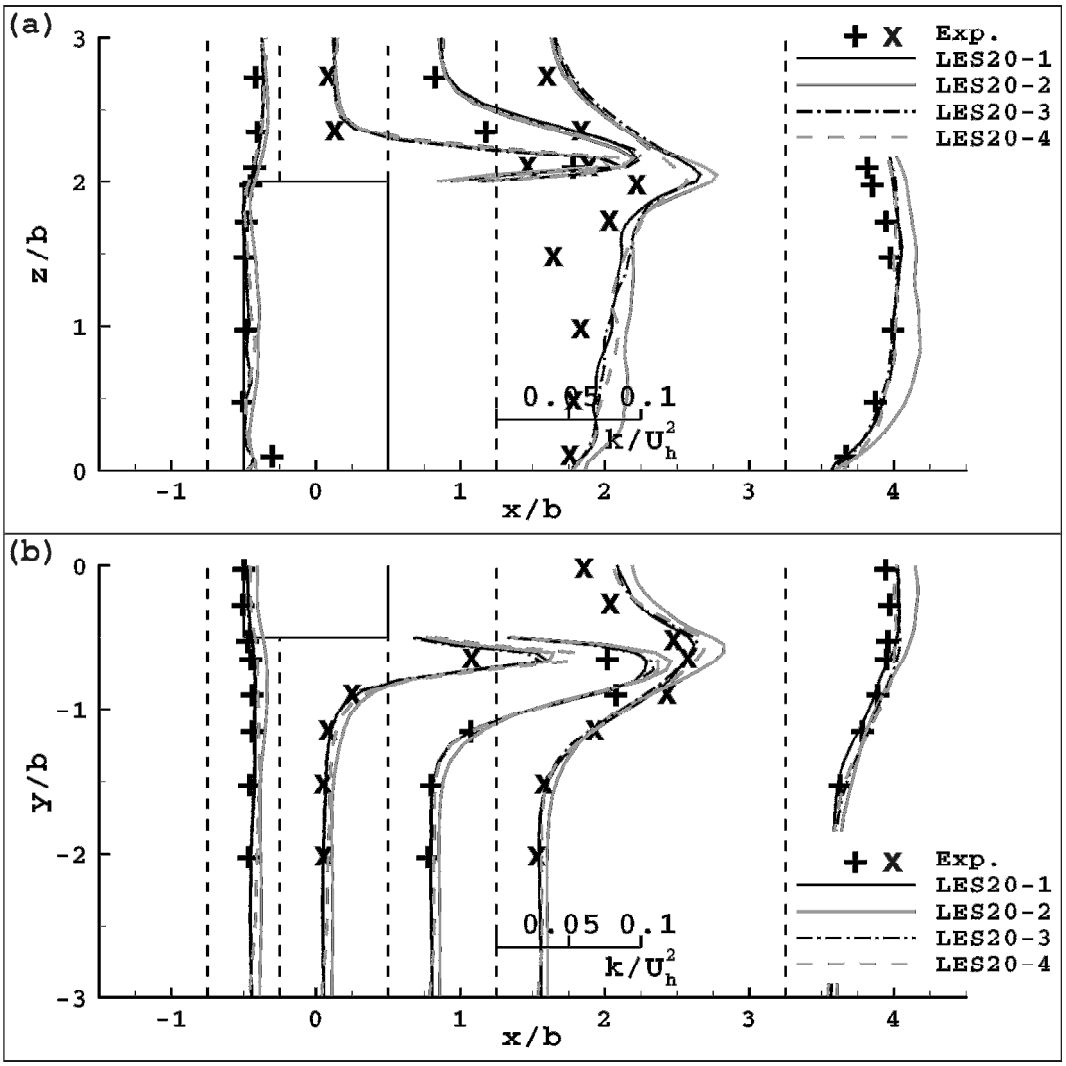

Figure 7. Influence of the SGS model: comparison between LES20-1 (C_s=0.1), LES20-2 (C_s=0.15), LES20-3 (dynamic) and LES20-4 (no SGS model). Experimental (symbols) and numerical (lines) profiles of non-dimensional turbulent kinetic energy in the planes (a) V0 and (b) H10.

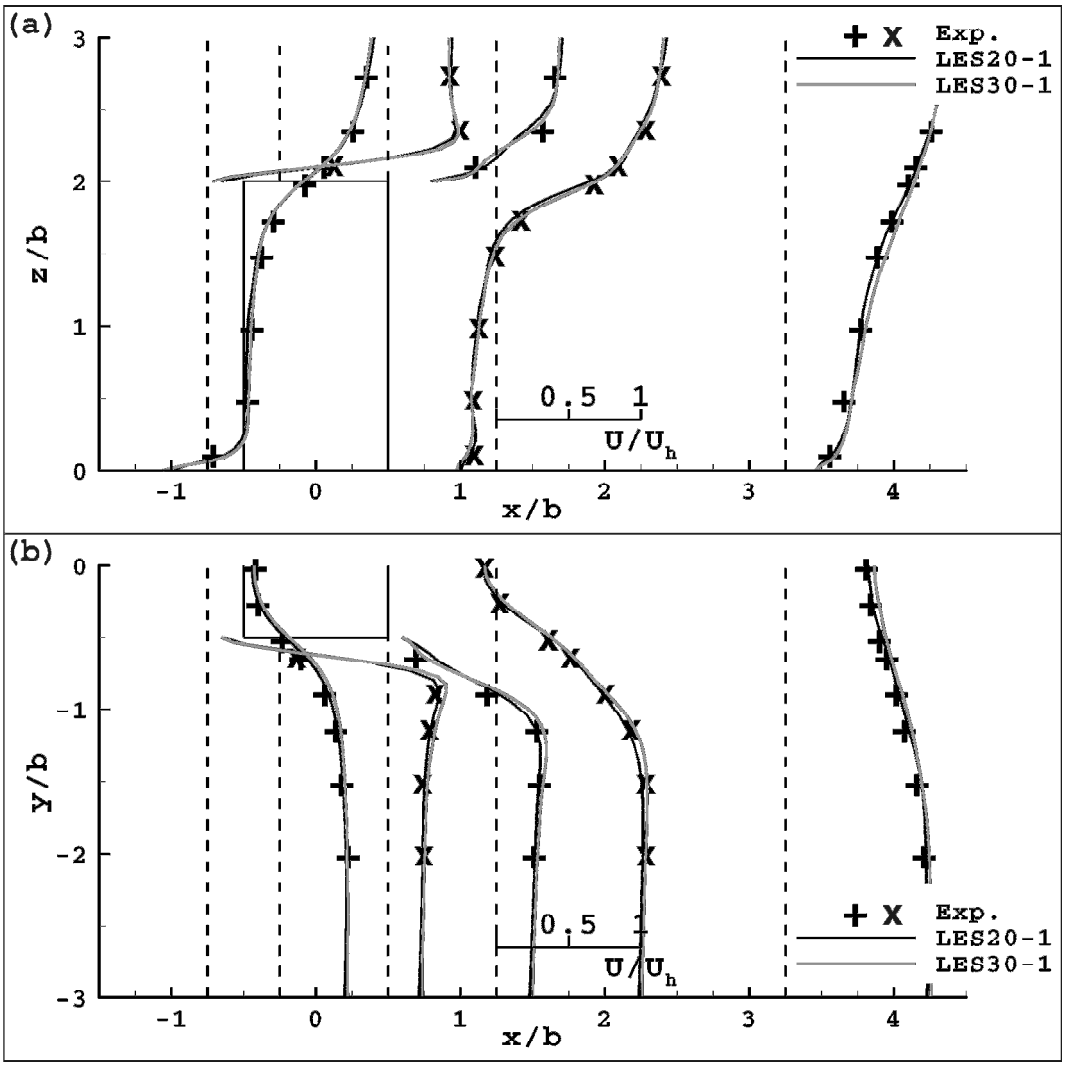

Figure 8. Influence of the grid resolution: comparison between LES20-1 and LES30-1. Experimental (symbols) and numerical (lines) profiles of non-dimensional mean streamwise velocity in the planes (a) V0 and (b) H10.

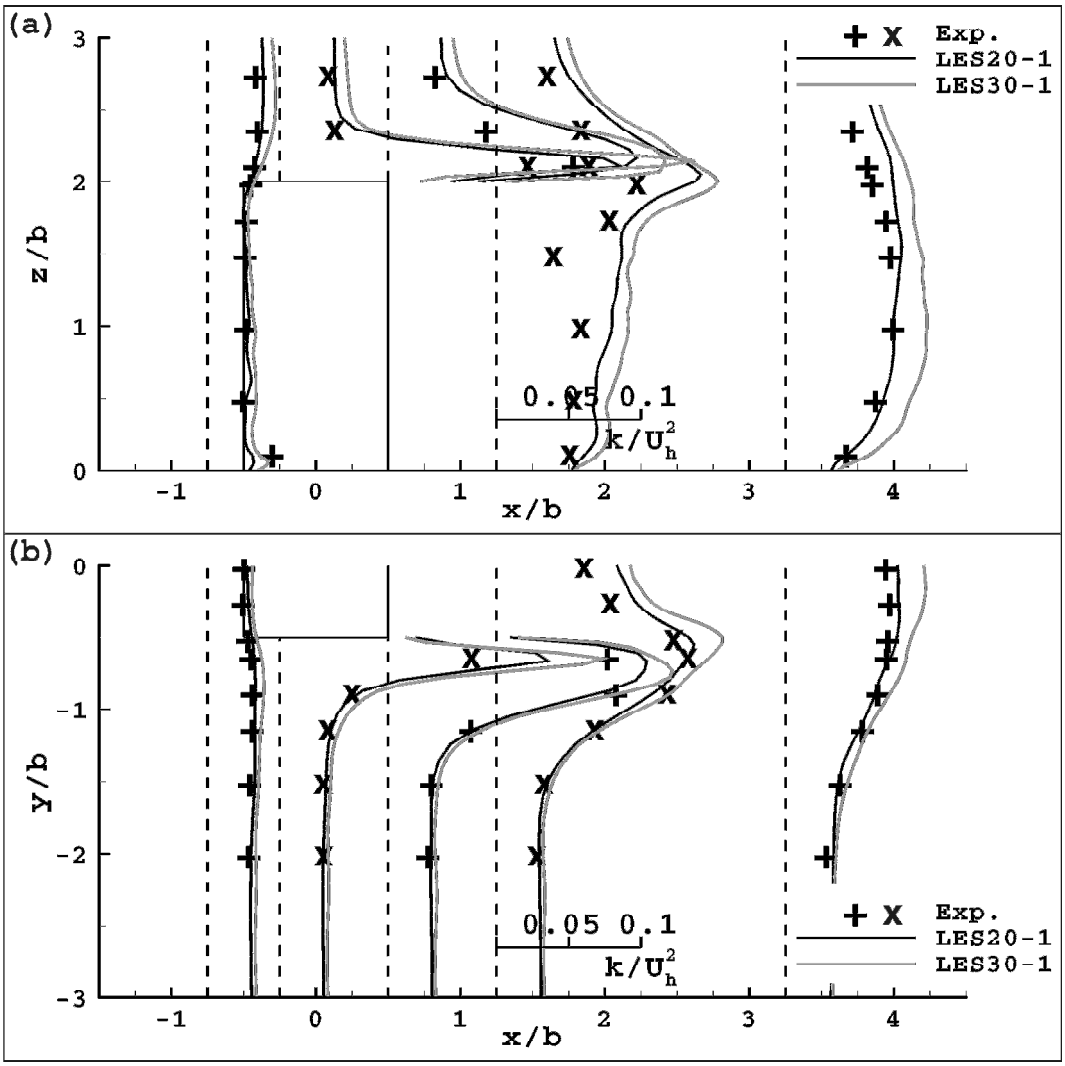

Figure 9. Influence of the grid resolution: comparison between LES20-1 and LES30-1. Experimental (symbols) and numerical (lines) profiles of non-dimensional turbulent kinetic energy in the planes (a) V0 and (b) H10.

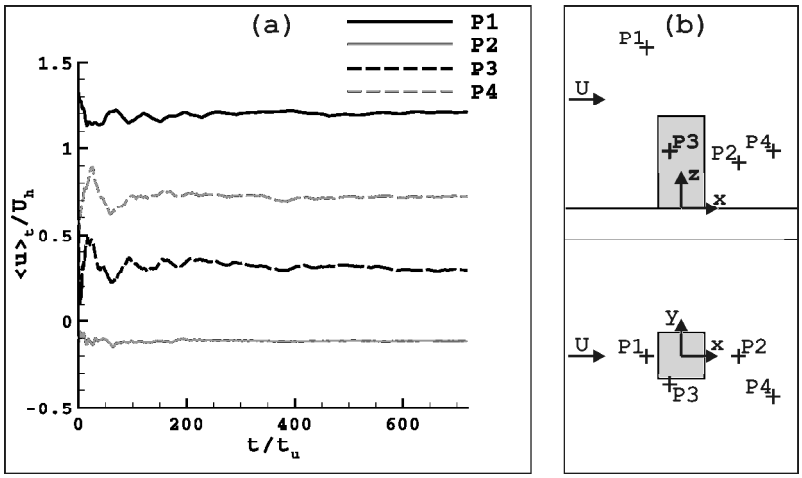

Figure 10. Convergence monitoring: (a) moving-average of the non-dimensional streamwise velocity at four monitoring points as a function of time in the averaging period for LES20-3. (b) Position of the monitoring points. Non-dimensional coordinates: P1 (-0.75; 0; 3.5); P2 (1.25; 0; 1); P3 (-0.25; -0.625; 1.25); P4 (2; -0.875; 1.25).

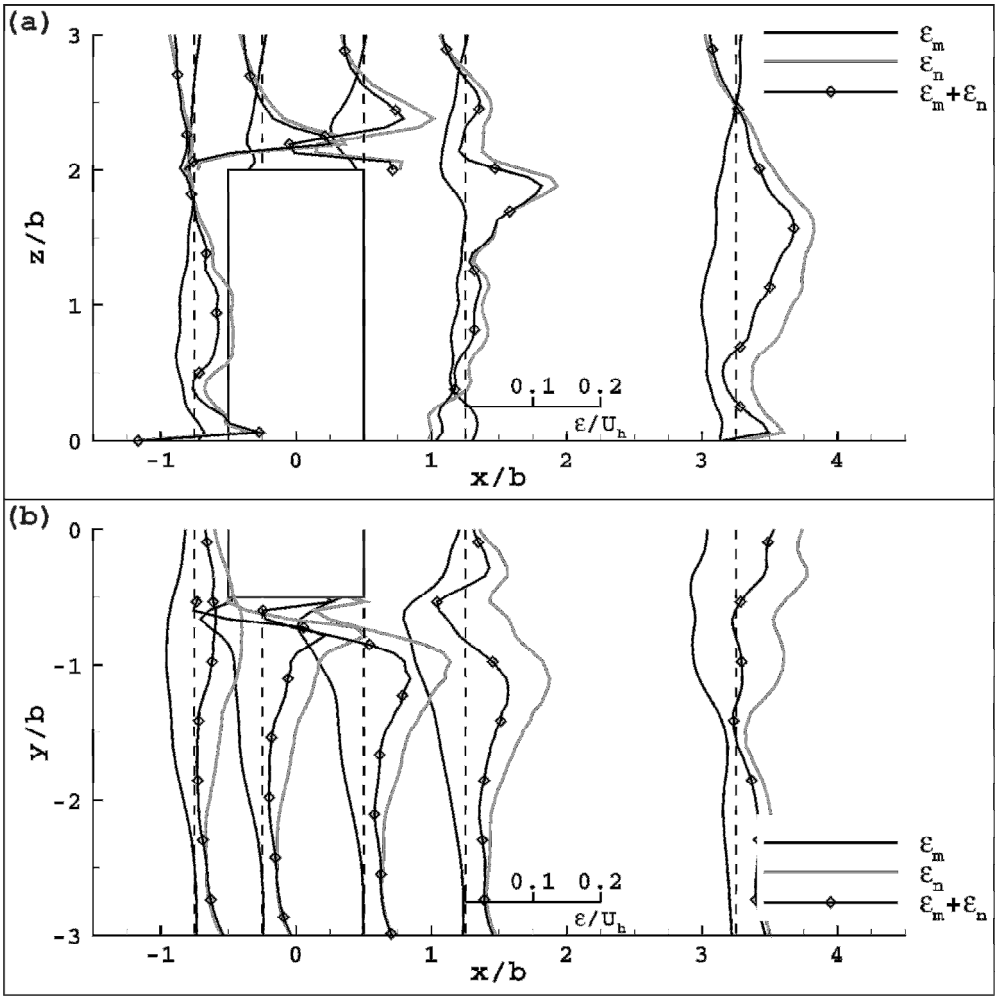

Figure 11. Results of SGMV technique for LES20-1: Estimation of the non-dimensional modeling, numerical and total error on mean streamwise velocity prediction in the planes (a) V0 and (b) H10.

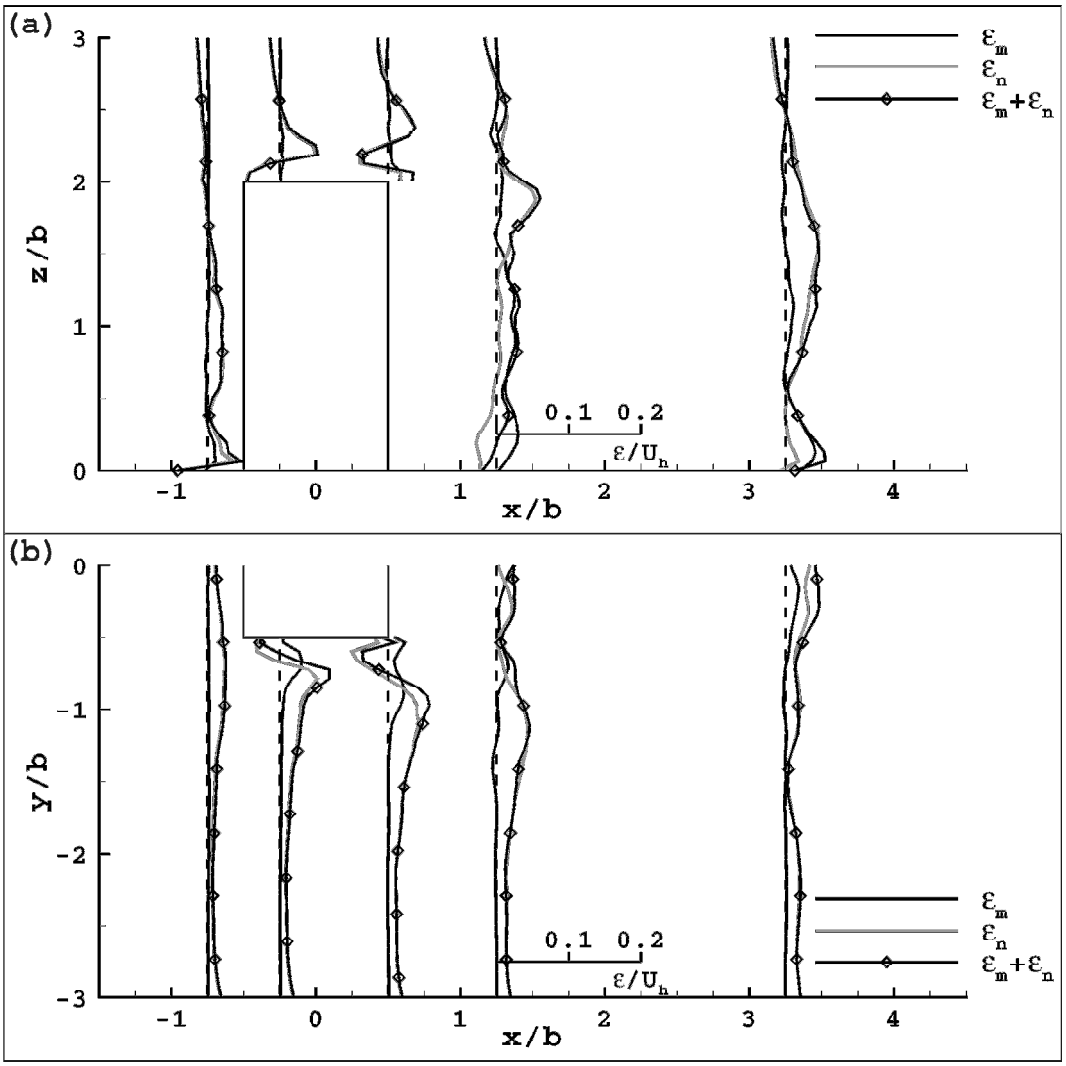

Figure 12. Results of SGMV technique for LES30-1: Estimation of the non-dimensional modeling, numerical and total error on mean streamwise velocity prediction in the planes (a) V0 and (b) H10.

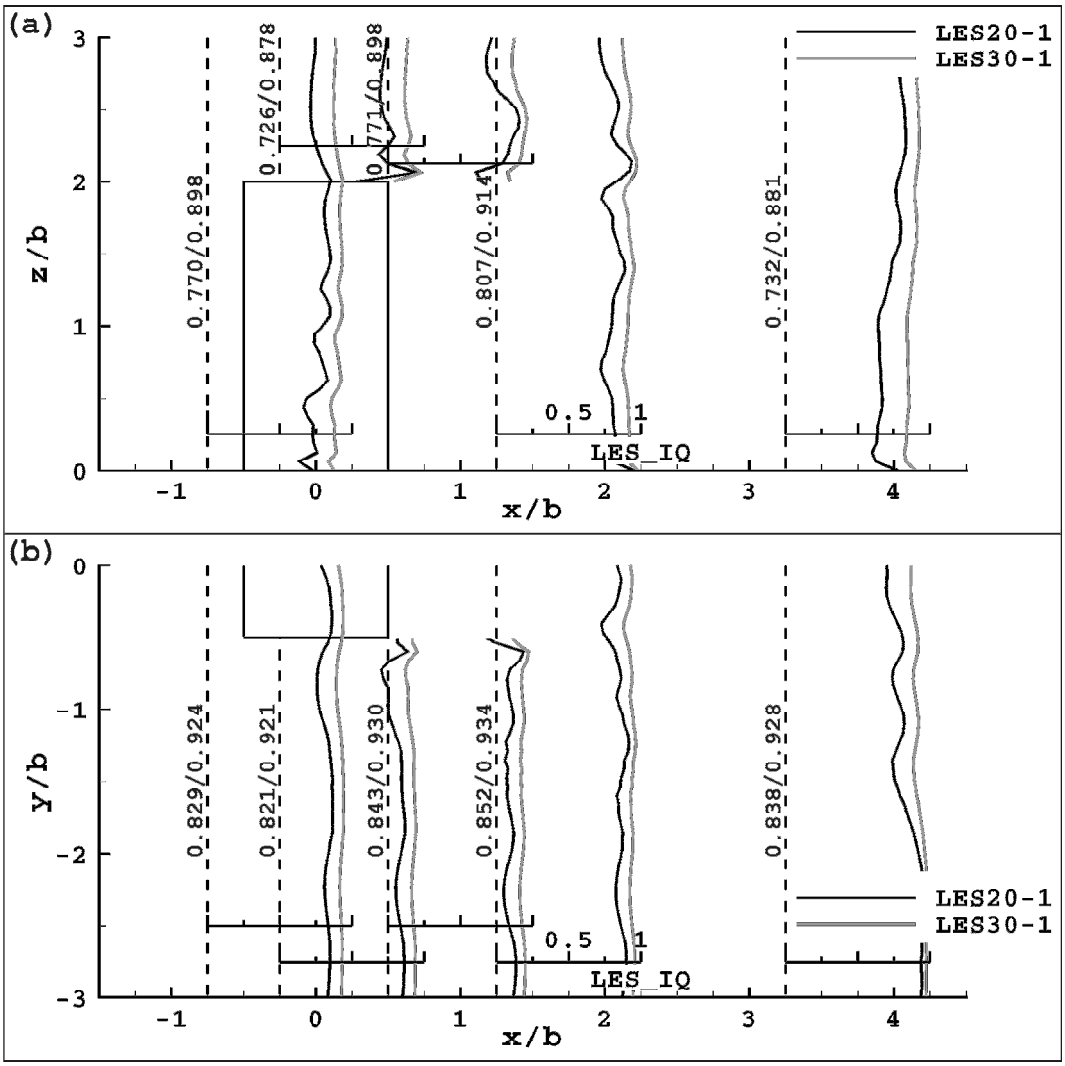

Figure 13. Profiles of *LES_IQ* for cases LES20-1 and LES30-1 in the planes (a) V0 and (b) H10. The values averaged on (a) $0<z/b<3$ and (b) $-3< y/b<0$ are indicated on each line (the first/lowest value corresponds to LES20-1 and the second/highest value to LES30-1).

Tables

Table 1. Characteristics of the two computational grids.

Name	Nb of cells: Total	Nb of cells: Building	Cell size: Building [m]	Cell size: Maximum [m]
Grid20	737,920	20×20×40	0.004	0.036
Grid30	2,504,160	30×30×60	0.0027	0.024

Table 2. List and description of the cases. VM indicates Vortex Method for inlet boundary condition.

Case	Grid	SGS model	Constant C_s	Inlet method
LES20-1	Grid20	Standard Smagorinsky	0.1	VM
LES20-2	Grid20	Standard Smagorinsky	0.15	VM
LES20-3	Grid20	Dynamic Smagorinsky	-	VM
LES20-4	Grid20	-	-	VM
LES20-5	Grid20	Standard Smagorinsky	0.1	No perturbation
LES30-1	Grid30	Standard Smagorinsky	0.1	VM
LES30-2	Grid30	Standard Smagorinsky	0.15	VM
LES30-3	Grid30	Dynamic Smagorinsky	-	VM
LES30-4	Grid30	-	-	VM

Table 3. Validation metrics (hit rate *q*, factor of two of observations *FAC2*, fractional bias *FB* and normalized mean square error *NMSE*) for the seven simulations. The metrics for *U* and *k* take into account the 186 measurement points while *V* is evaluated in the planes H1 and H10 and *W* in the plane V0. Thresholds for *q*: D_q=0.25; W_q=0.03 for *U*, *V* and *W*. D_q=0.25; W_q=0.003 for *k*.

	U/U_h		V/U_h (planes H1 & H10)		W/U_h (plane V0)		k/U_h^2			
	q	FAC2	q	FAC2	q	FAC2	q	FAC2	FB	NMSE
Ideal value	1	1	1	1	1	1	1	1	0	0
LES20-1	0.90	0.96	0.78	0.73	0.71	0.76	0.65	0.98	-0.16	0.10
LES20-2	0.87	0.94	0.77	0.76	0.70	0.79	0.34	0.98	-0.28	0.16
LES20-3	0.89	0.95	0.84	0.75	0.73	0.76	0.66	0.99	-0.17	0.10
LES20-4	0.90	0.96	0.86	0.72	0.65	0.77	0.57	0.99	-0.20	0.11
LES20-5	0.84	0.95	0.88	0.74	0.50	0.70	0.17	0.43	0.69	0.67
LES30-1	0.90	0.96	0.67	0.77	0.62	0.74	0.32	0.98	-0.30	0.19
LES30-2	0.86	0.93	0.71	0.79	0.64	0.76	0.32	0.98	-0.29	0.17
LES30-3	0.90	0.95	0.80	0.76	0.71	0.82	0.16	0.96	-0.33	0.20
LES30-4	0.91	0.95	0.80	0.79	0.65	0.76	0.36	0.98	-0.28	0.18

Table 4. Non-dimensional length of the rooftop (X_r/b) and wake (X_w/b) recirculation zones. Results from (Tominaga et al., 2008) correspond to "Case 2", with inflow turbulence obtained from a precursor simulation.

Case	X_r/b	X_W/b
Exp. (Meng and Hibi, 1998)	0.52	1.42
Tominaga et al., 2008	0.50	2.10
LES20-1	0.59	1.65
LES20-2	0.59	1.66
LES20-3	0.60	1.65
LES20-4	0.61	1.57
LES20-5	0.75	1.89
LES30-1	0.59	1.78
LES30-2	0.62	1.90
LES30-3	0.57	1.74
LES30-3	0.57	1.60

Table 5. Convergence monitoring on LES20-3: e_{conv} (%) at P1, P2, P3 and P4 for eight successive equal ranges of time steps in the averaging period. Total number of time steps in the averaging period: 16,000.

point / range of time steps	P1	P2	P3	P4
1-2000	15.8	74.7	182.5	49.8
2001-4000	4.3	11.5	27.4	6.7
4001-6000	2.5	10.6	15.9	3.3
6001-8000	1.3	7.0	13.8	3.5
8001-10000	1.5	4.5	10.0	3.3
10001-12000	1.0	3.8	5.1	1.5
12001-14000	1.0	5.1	7.9	1.6
14001-16000	0.5	3.8	4.1	1.1